LETTER • OPEN ACCESS

Micrometeorological impacts of offshore wind farms as seen in observations and simulations

View the article online for updates and enhancements.

Environmental Research Letters

LETTER

Micrometeorological impacts of offshore wind farms as seen in observations and simulations

S K Siedersleben[1] , J K Lundquist[2,3] , A Platis[4] , J Bange[4], K Bärfuss[5], A Lampert[5], B Cañadillas[6],
T Neumann[6] and S Emeis[1]

[1] Karlsruhe Institute of Technology, Institute of Meteorology and Climate Research, Atmospheric Environmental Research (IMK-IFU), Germany
[2] University of Colorado, Department of Atmospheric and Oceanic Sciences, Boulder, Colorado, United States of America
[3] National Renewable Energy Laboratory, Golden, Colorado, United States of America
[4] Environmental Physics, ZAG, University of Tübingen, Germany
[5] Institute of Flight Guidance, Technische Universität Braunschweig, Germany
[6] UL International GmbH, Germany

E-mail: simon.siedersleben@kit.edu

Abstract

In Europe, offshore wind farms have a capacity of 16 GW, with 71% installed at the North Sea. These wind farms represent an additional source of turbulence and may influence the stratification of the marine boundary layer. We present aircraft measurements and simulations showing an impact on temperature and humidity at hub height in the order of 0.5 K and 0.5 g kg^{-1} even 60 km downwind of a wind farm cluster. We extend these simulations to explore a realistic future scenario, suggesting wakes in potential temperature and water vapor propagating more than 100 km downwind. Such impacts of wind farms are only observed in case of a strong stable stratification at rotor height, allowing wind farms to mix warmer air downward.

1. Introduction

The offshore wind energy market grew rapidly in the year 2017—compared to the year 2016, 2.6 times more wind farms were installed offshore in Europe. Almost 85% of these wind farms were installed in the North Sea (WindEurope 2017). These investments are motivated by the stronger and steadier winds in the North Sea compared to onshore sites (Bilgili *et al* 2011) as well as relatively shallow water depth in the North Sea (WindEurope 2017).

On- and offshore wind farms can affect the micro-meteorology of the boundary layer. Wakes generated by single wind turbines reduce momentum downwind, resulting in a wind speed deficit (e.g. Lissaman 1979, Barthelmie *et al* 2010, Hirth and Schroeder 2013, Rhodes and Lundquist 2013, Djath *et al* 2018). Christiansen and Hasager (2005) observed offshore wakes via sythetic aperture radar satellite images and showed that these wakes can propagate 20 km downwind. These results were confirmed,

recently, by airborne measurements taken downwind of large offshore wind farms at the North Sea (Platis *et al* 2018). During stable atmospheric conditions, these offshore wakes can be longer than 70 km at offshore sites (Platis *et al* 2018).

Onshore wind farms can impact the boundary layer (e.g. Baidya Roy and Traiteur 2010, Zhou *et al* 2012, Rajewski *et al* 2013, Smith *et al* 2013, Rajewski *et al* 2014, Armstrong *et al* 2016). For example, Zhou *et al* (2012) observed a warming of 0.5 K in the vicinity of onshore wind farms, especially during nocturnal stable conditions. Therefore, the implications of onshore wind farms on agriculture are discussed (e.g. Baidya Roy and Traiteur 2010, Rajewski *et al* 2013, Smith *et al* 2013, Zhang *et al* 2013).

Most offshore observational studies have so far generally focused on the wind and power deficit observed in and downwind of large wind farms (e.g. Barthelmie *et al* 2010, Nygaard 2014, Nygaard and Hansen 2016) except Foreman *et al* (2017). Only few studies have investigated the potential effect of wind

farms on the marine boundary layer (MBL). These studies were motivated by visible cloud effects as they were seen in photos taken at a wind farm at the coast of Denmark (Emeis 2010, Hasager *et al* 2013, 2017), indicating fog formation and dispersion due to enhanced mixing downwind of wind farms. Associated with enhanced mixing, Foreman *et al* (2017) reported a decreased sensible heat flux downwind of a small offshore wind farm during stable conditions in the North Sea.

Modeling studies suggest a change in temperature and moisture downwind of offshore wind farms. Vautard *et al* (2014) obtained increased temperatures at the North Sea in the area of offshore wind farms in their simulations. In contrast, Wang and Prinn (2011) and Huang and Hall (2015) reported a potential cooling effect in the vicinity of offshore wind farms due to an increased latent heat flux, although Wang and Prinn (2011) represented the offshore wind farms as areas of increased surface roughness. Fitch *et al* (2013) showed that this roughness approach is not suitable to investigate climate impacts. However, no field measurements have so far investigated this potential cooling or warming effect.

Herein, we present aircraft observations accompanied with mesoscale simulations to provide a first look into spatial dimensions of these important impacts. Within the research project WIPAFF (Emeis *et al* 2016), 26 flights were conducted in the far field of wind farm clusters. During *nine* flights we observed differences between potential temperature and/or water vapor concentration within and outside of the wake. Herein, we present one case study in detail and compare this case to the remaining 25 aircraft measurements to identify atmospheric conditions that favor thermodynamic impacts of wind farms on the MBL. We present these impacts to constrain maximal possible impacts of offshore wind farms on the MBL. We want to answer the following questions:

- How large are the micrometeorological impacts of offshore wind farms on the MBL?
- How is the micrometeorological impact caused?
- What is the influence of existing and planned offshore wind farms on the MBL at the North Sea?

In section 2, we present the model configuration and the aircraft observations used to determine the impacts of wind farms on the MBL. In section 3 we compare the observation to our simulations up- and downwind of the wind farms. A discussion in section 4.1 compares cases with impacts on temperature with cases having no impact. Further, we suggest vertical profiles under which an impact on the MBL can be expected. Section 4.2 addresses the implications of our results with respect to existing and planned

offshore wind farms. This study ends with a conclusion (section 5).

2. Data and method

2.1. Numerical simulations

The numerical setup and the parameterizations in this study are the same as in Siedersleben *et al* (2018); the reader is referred to this paper for full details. Numerical simulations are performed with Weather Research and Forecasting model WRF 3.8.1 (Skamarock *et al* 2008) with three domains having a resolution of 15, 5 and 1.67 km (figure 1), resulting in up to six wind turbines per grid cell. ECMWF analysis data provide the initial and the boundary condition for the simulation. The model uses 50 vertical levels, with a spacing of ≈ 35 m at the bottom with the lowest level at 17 m above mean sea level, resulting in one level below rotor height and three levels intersecting with the rotor area (figure 2).

We use the wind farm parameterization (WFP) of Fitch *et al* (2012) to simulate the interaction between atmosphere and wind farms. The WFP extracts kinetic energy from the mean flow and acts as a source of turbulence, depending on the thrust and power coefficients of the installed turbines in the model (Fitch *et al* 2012, Jiménez *et al* 2015, Lee and Lundquist 2017). Therefore, the WFP interacts with the planetary boundary layer scheme of Nakanishi and Niino (2004) that we use in all three domains.

We focus mainly on wakes generated by a wind farm cluster consisting of the wind farms Meerwind-Sued|Ost, Nordsee Ost and Amrumbank West (see close-up, figure 1). The observations conducted on 10 September 2016 were carried out at this wind farm cluster. These three wind farms have two turbine types: SIEMENS SWT 3.6-120 and SENVION 6.2, with 90 and 95 m hub heights and rotor diameters of 120 and 126 m. The thrust and power coefficients of these wind farms are not available to the public. Therefore, we use the coefficients of the wind turbine Siemens SWT 3.6-120-onshore as these are available (http://wind-turbine-models.com/turbines/646-siemens-swt-3.6-120-shore (30 October 2018)). We have shown in Siedersleben *et al* (2018) that the errors introduced by these uncertainties have only a marginal effect on the wake effect.

Additional simulations include all approved offshore wind farms under construction at the North Sea (i.e. all blue and orange wind farms shown in figure 1). For these simulations we assume the same wind turbine type for simplicity, the SIEMENS SWT 3.6-120. To assess the overall impact of these wind farms at the North Sea, we conducted a second simulation with the WFP switched off. We refer to the simulations without wind farms as no wind farm simulation (NWF) and to the ones using the WFP as wind farm simulation (WF).
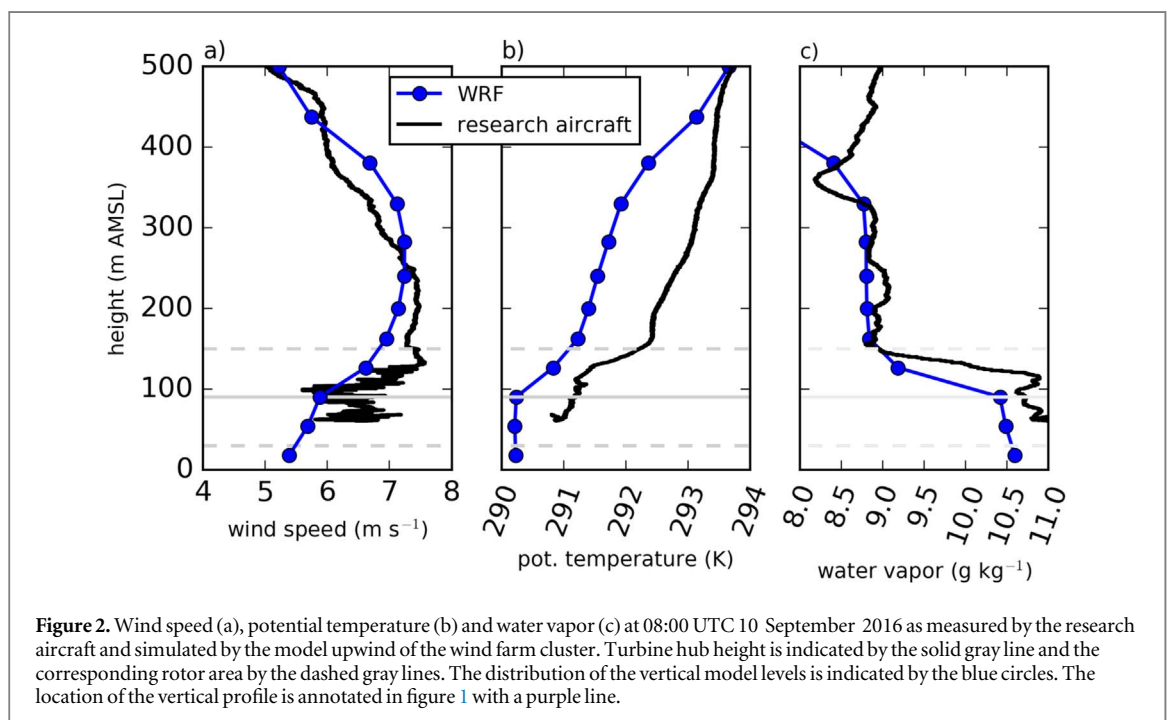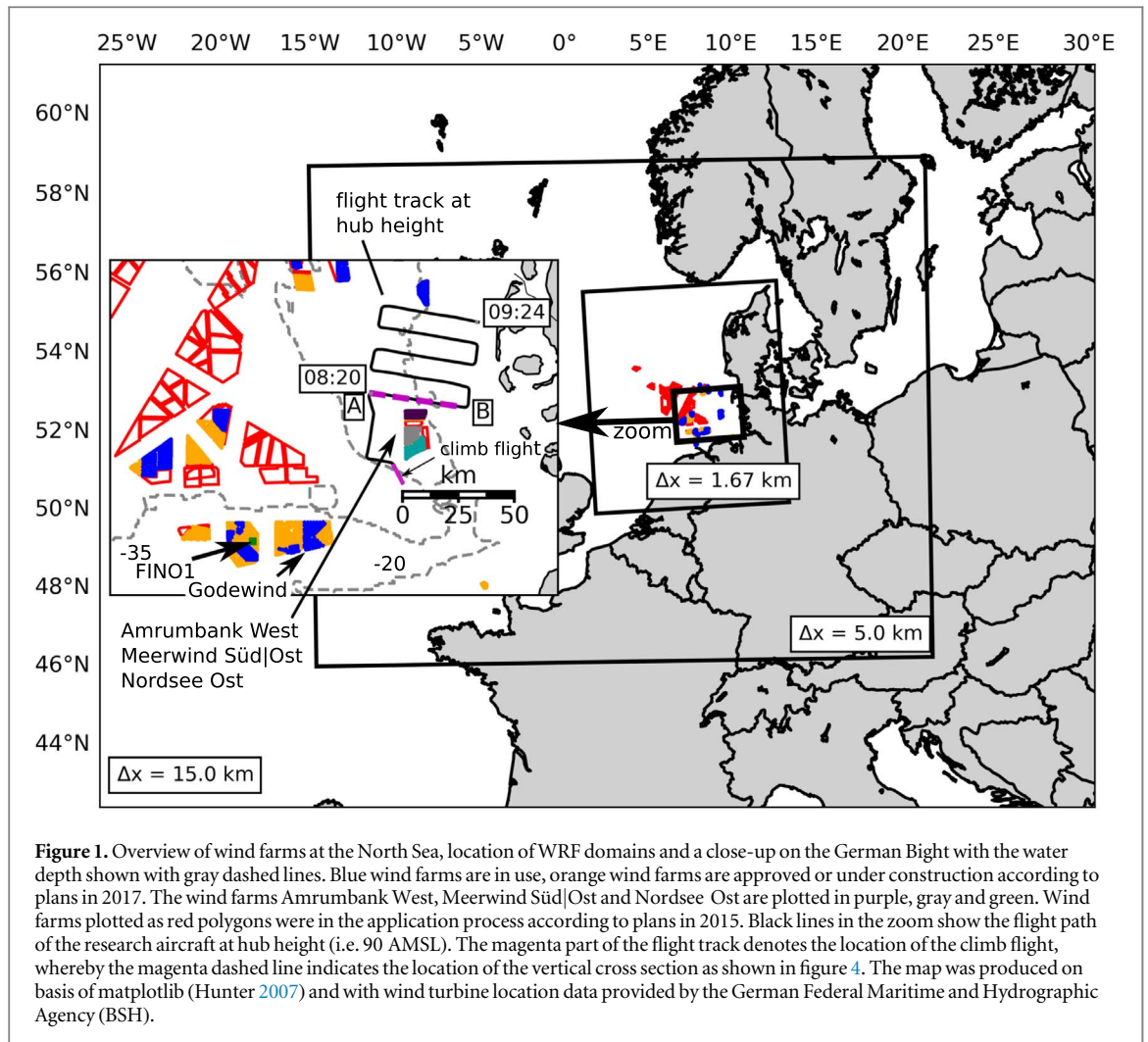
Figure 1. Overview of wind farms at the North Sea, location of WRF domains and a close-up on the German Bight with the water depth shown with gray dashed lines. Blue wind farms are in use, orange wind farms are approved or under construction according to plans in 2017. The wind farms Amrumbank West, Meerwind Süd|Ost and Nordsee Ost are plotted in purple, gray and green. Wind farms plotted as red polygons were in the application process according to plans in 2015. Black lines in the zoom show the flight path of the research aircraft at hub height (i.e. 90 AMSL). The magenta part of the flight track denotes the location of the climb flight, whereby the magenta dashed line indicates the location of the vertical cross section as shown in figure 4. The map was produced on basis of matplotlib (Hunter 2007) and with wind turbine location data provided by the German Federal Maritime and Hydrographic Agency (BSH).

Figure 2. Wind speed (a), potential temperature (b) and water vapor (c) at 08:00 UTC 10 September 2016 as measured by the research aircraft and simulated by the model upwind of the wind farm cluster. Turbine hub height is indicated by the solid gray line and the corresponding rotor area by the dashed gray lines. The distribution of the vertical model levels is indicated by the blue circles. The location of the vertical profile is annotated in figure 1 with a purple line.

Table 1. Overview of flights conducted within the WIPAFF project downwind of large offshore wind farms. The numbering of the aircraft measurements corresponds to the numbering in figures 5 and 6. The letters A and G indicate the measurement location; A refers the to wind farm cluster consisting of Amrumbank West, Meerwind Sued|Ost and Nordsee Ost and G for the wind farm Godewind. The locations of these wind farms are indicated in figure 1. The column indicated with wsp, shows the measured wind speed at hub height according to figure 5. The sixth and seventh column indicate whether the wind farms had an impact on temperature or humidity at hub height downwind. The atmospheric stability during each measurement is shown in the last column according to the potential temperature gradient within the rotor area shown in figure 5. Observations where wind farms had an impact on the atmosphere are listed at the beginning of the table.

Index	Date	Time (UTC)	Wind farm	wsp (m s^{-1})	Θ	Humidity	Stability
(a)	6 September 2016	14:13–17:20	A	6–9	Warming	Drying	Stable
(b)	10 September 2016	07:30–11:15	A	6.5	Warming	Drying	Stable
(c)	11 April 2017	14:04–18:00	G	12	Warming	Drying	Stable
(d)	8 August 2017	08:35–12:35	A	7	Warming	Drying	Stable
(e)	17 August 2017	06:06–10:10	A	10	Warming	Drying	Stable
(f)	30 March 2017	13:57–17:02	G	11.5	None	Humidification	Stable
(g)	17 May 2017	15:16–19:22	A	13.5	Cooling	None	Stable
(h)	27 May 2017	07:57–11:58	A	8.2	Cooling	None	Stable
(i)	27 May 2017	12:39–16:36	A	11	Cooling	Drying	Stable
(j)	31 March 2017	13:36–17:00	G	11	None	None	Stable
(k)	24 May 2017	11:40–09:34	G	7.5	None	None	Stable
(l)	7 September 2016	07:30–10:45	A	5.5	None	None	Stable
(m)	7 September 2016	12:00–14:00	A	4.5	None	None	Stable
(n)	8 September 2016	08:30–12:30	A	7	None	None	Unclear
(o)	9 September 2016	13:42–17:17	A and G	7	None	None	Neutral
(p)	10 September 2016	12:15–16:00	A	4.5	None	None	Stable
(q)	5 April 2017	13:42–14:34	G	12	None	None	Neutral
(r)	6 April 2017	13:29–16:22	G	8	None	None	Neutral
(s)	9 April 2017	11:36–14:07	G	4	None	None	Stable
(t)	9 April 2017	14:32–18:12	G	3	None	None	Stable
(u)	13 April 2017	11:35–15:39	G	13	None	None	Neutral
(v)	23 May 2017	09:00–10:30	G	5	None	None	Stable
(w)	23 May 2017	11:18–15:00	A	11.5	None	None	Unclear
(x)	1 June 2017	06:55–10:54	A	8.0	None	None	Neutral
(y)	14 August 2017	14:40–18:31	A	8.8	None	None	Neutral
(z)	15 October 2017	11:52–15:35	G	8.5	None	None	Neutral

2.2. Aircraft measurements

As part of the research project Wind Park Far Field (WIPAFF) (Emeis *et al* 2016), 26 flights were conducted in the far field of large offshore wind farm clusters at the North Sea from September 2016 to October 2017 (Platis *et al* 2018) (see table 1 for a overview). During *eight* flights in this project we observed a change in temperature and/or humidity within the wake of a wind farm cluster; one case is difficult to interpret and will be discussed in section 4. We will focus on aircraft measurements conducted on 10 September 2016 from 08:00 to 11:00 UTC and then compare the results against 25 other flights.

On 10 September 2016, the aircraft (Dornier DO–128 of TU Braunschweig) sampled the wind vector, humidity, pressure and temperature at 100 Hz (Platis *et al* 2018) along the flight path (figure 1). The aircraft flew the first flight leg (identical to the location of cross-section A–B) 5 km downwind of the last turbine at hub height, followed by four further flight legs, located 15, 25, 35 and 45 km downwind of the wind farm cluster—also at hub height. This horizontal flight pattern started at 08:20 UTC and ended at 09:24 UTC (see annotations figure 1).

Besides the measurements at hub height downwind, the aircraft conducted measurements along the vertical cross-section indicated with A, B in figure 1. The aircraft flew at five different heights, starting at 60 m AMSL followed by measurements at 90, 120, 150, and 220 m AMSL along the vertical A–B. With these measurements, we investigate the effect of large offshore wind farms on the stratification of the MBL. The measurements along vertical A–B started at 10:00 UTC and ended at 11:00 UTC.
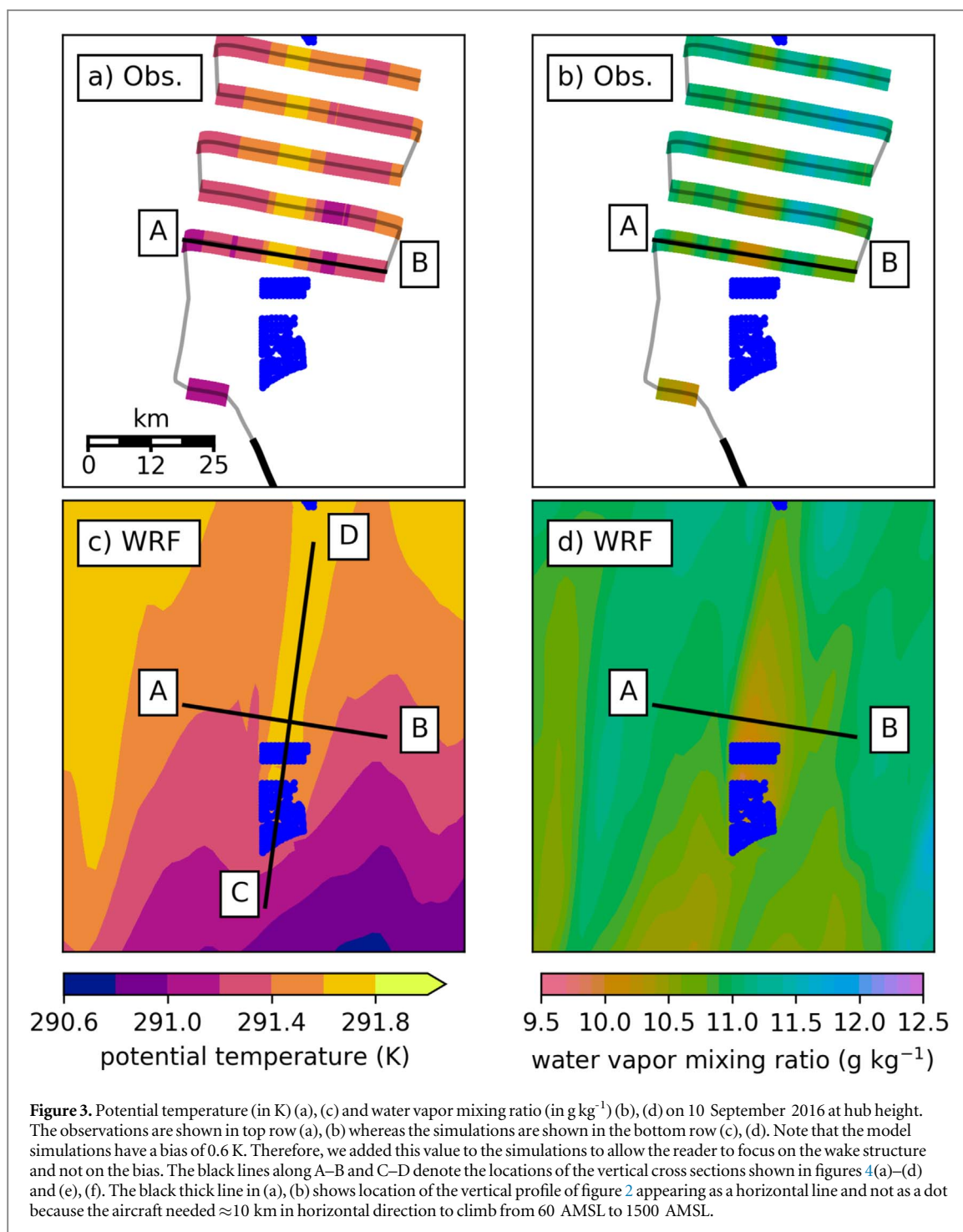
The aircraft probed the atmosphere 5 km upwind of the wind farm cluster to quantify the upwind conditions at 08:00 UTC (see location in figure 1).

3. Impacts on temperature and water vapor on 10 September 2016

First the model is compared upwind of the wind farms to the aircraft measurements (section 3.1) before the impact of wind farms on temperature and water vapor is evaluated in sections 3.2 and 3.3.

3.1. Stratification of the atmosphere upwind of the wind farm cluster

The atmosphere upwind of the wind farms was stably stratified at 08:00 UTC 10 September 2016 (figures 2(a)–(c)). From hub-height at 90 m to the top of the rotor

Figure 3. Potential temperature (in K) (a), (c) and water vapor mixing ratio (in g kg^{-1}) (b), (d) on 10 September 2016 at hub height. The observations are shown in top row (a), (b) whereas the simulations are shown in the bottom row (c), (d). Note that the model simulations have a bias of 0.6 K. Therefore, we added this value to the simulations to allow the reader to focus on the wake structure and not on the bias. The black lines along A–B and C–D denote the locations of the vertical cross sections shown in figures 4(a)–(d) and (e), (f). The black thick line in (a), (b) shows location of the vertical profile of figure 2 appearing as a horizontal line and not as a dot because the aircraft needed ≈10 km in horizontal direction to climb from 60 AMSL to 1500 AMSL.

disk at 150 m, an inversion is visible associated with a decreasing water vapor mixing ratio from 11.0 to 8.5 g kg^{-1}. The model simulates the upwind conditions reasonably well, showing a clear inversion starting at hub height and the associated decreasing water vapor concentration. However, the model has a constant cool bias between 0.6 and 1 K. This deviation is mainly caused by an overestimated nocturnal cooling on the land upwind (Siedersleben *et al* 2018).

3.2. Temperature
Behind the wind farms, warmer air was observed and simulated at hub height within the wake even 45 km downwind of the last turbine (figures 3(a) and (c)). According to the simulations, potential temperature in the wake is 0.4 K warmer than the air upwind. This effect is more pronounced in the observations. At hub height in the upwind climb flight, a potential temperature of 291.2 K was measured (figure 2) compared to maximal 291.8 K within the wake, indicating a warming of up to 0.6 K at hub height. Additionally, the observations show a stronger horizontal difference between wake and no-wake region downwind of the wind farm cluster. At the eastern flank a potential temperature gradient of 0.8 K was observed, in contrast to a difference of 0.4 K in the simulations.

The model has a cold bias of ≈ 0.6 K compared to the observations. However, the model is stably-stratified above hub height, corresponding to the observations (more details in Siedersleben *et al* (2018)). As we want to investigate the impact of wind farms on the MBL and not the bias of the simulations, we add 0.6 K to all shown potential temperature figures in this study.

The potential temperature wake was associated with a mixed layer, as seen in the cross-section 5 km downwind of the wind farm cluster (figures 4(a) and (c)). However, both cross-sections from observation and simulation indicate that warmer air was mixed downward. The mixed layer extends up to 120 m AMSL in the observations (figure 4(a)); in the simulation this neutral layer is only 100 m thick.

Mixing warmer air downward corresponds to an enhanced sensible heat flux downward (figure 4(e)). In the observations, the atmosphere was stably stratified, consequently, we expect a sensible heat flux towards the surface (i.e. a negative sensible heat flux). Figure 4(e) shows the difference in sensible heat flux between a WF and a NWF simulation along the cross-section C–D. The blue contours indicate that the wind farms caused a greater downward heat flux above and within the farm, hence, explaining the warming below ≈ 180 m AMSL (figure 4(e)). The simulations show cooling aloft right above the farm area and warming within the farms but starting half-way through the farm area and extending much farther downwind than the cooler area figure (4(f)).

3.3. Water vapor
Within the wake of the wind farm cluster the air is dryer than in the ambient air outside of the wake (figures 3(b) and (d)). Similar to the wake in the potential temperature, the dryer air is still visible 45 km downwind of the wind farm cluster. Within the wake region the air has a minimum water vapor mixing ratio of 9.8 g kg^{-1} compared to maximal values of 11.8 g kg^{-1} outside of the wake. Corresponding to the observations, the model simulates dryer air within the wake region with values around 9.8 g kg^{-1}. However, the simulations suggest lower water vapor mixing ratios to the west of the wake. The observations show values up to 11.5 g kg^{-1} whereas the model predicts values in the order of 11 g kg^{-1} (figure 3(b)).

Associated with the neutrally-stratified layer, dryer air is evident in the vertical cross-section A–B (figures 4(b) and (d)) 5 km downwind of the wind farm cluster. Similar to the potential temperature, it is most likely that the dryer air originated from the dryer layer aloft above 150 m AMSL. This height corresponds to the upper limit of the rotor area, emphasizing that air stemming from above the rotor area is mixed downwards. The mixing of air above the rotor area seems to be be more pronounced in the model than in the observation. Within the upper rotor area, the model simulates a water vapor

concentration of 9.5 g kg^{-1}, whereby the observations show concentrations in the order of 10.2 g kg^{-1}, indicating that dry air was entrained into too low elevations, due to enhanced vertical mixing into the farms as described in (e.g. Abkar and Porté-Agel 2015, Pan and Archer 2018).

4. Discussion

This discussion section consists of two parts: the first part discusses the results of the presented case study compared to the other 25 aircraft measurements. The second part estimates the effect of all installed and planned offshore wind farms (i.e. blue and orange wind farms in figure 1) on the MBL for the 10 September 2016 case.

4.1. Comparison to other cases
Given the results from the case study of the 10 September 2016, one could draw the conclusion that stable conditions are a sufficient constraint to observe a warming and drying at hub height downwind of large offshore wind farms However, this assumption does not hold when analyzing the remaining 25 cases. For example, in the afternoon of the 10 September 2016, the aircraft flew a similar pattern as shown in figure 3, but did not observe any change in temperature and humidity although the atmosphere was stably stratified at hub height (figure 5(p)). The vertical profiles taken in the morning and in the afternoon differ mainly in terms of wind speed. In the afternoon the wind speed at hub height decreased from 7 m s^{-1} to values below 6 m s^{-1} compared to the measurements in the morning, suggesting that the wind speed has to be above a certain threshold to generate enough turbulence to mix the air and induce a warming or drying. Applying these two constraints—stable conditions and wind speeds over 6 m s^{-1} at hub height to all 26 cases, eleven cases fulfill both criteria. Indeed, in eight of the eleven cases we observe a change in temperature (figure 6). In two of the remaining cases we cannot state for certain that a temperature change did not occur. In the first case (figure 6(f)) we have a strong background gradient in potential temperature hindering the observation of a change in temperature. In the second case ((j), not shown) we have only measurements along the wake and, hence, can not measure any difference between wake and none wake air. In the third case ((k), not shown) we did not observe an impact on temperature, despite the fact that the wind speed was above our defined threshold of 6 m s^{-1} and the atmosphere was stably stratified at rotor height (figure 5(k)). However, the measurements were conducted downwind of Godewind (see location in figure 1), a wind farm with fewer wind turbines than the wind farm cluster around Amrumbank West. Consequently, higher wind speeds are necessary to achieve the same amount of mixing. Therefore, we
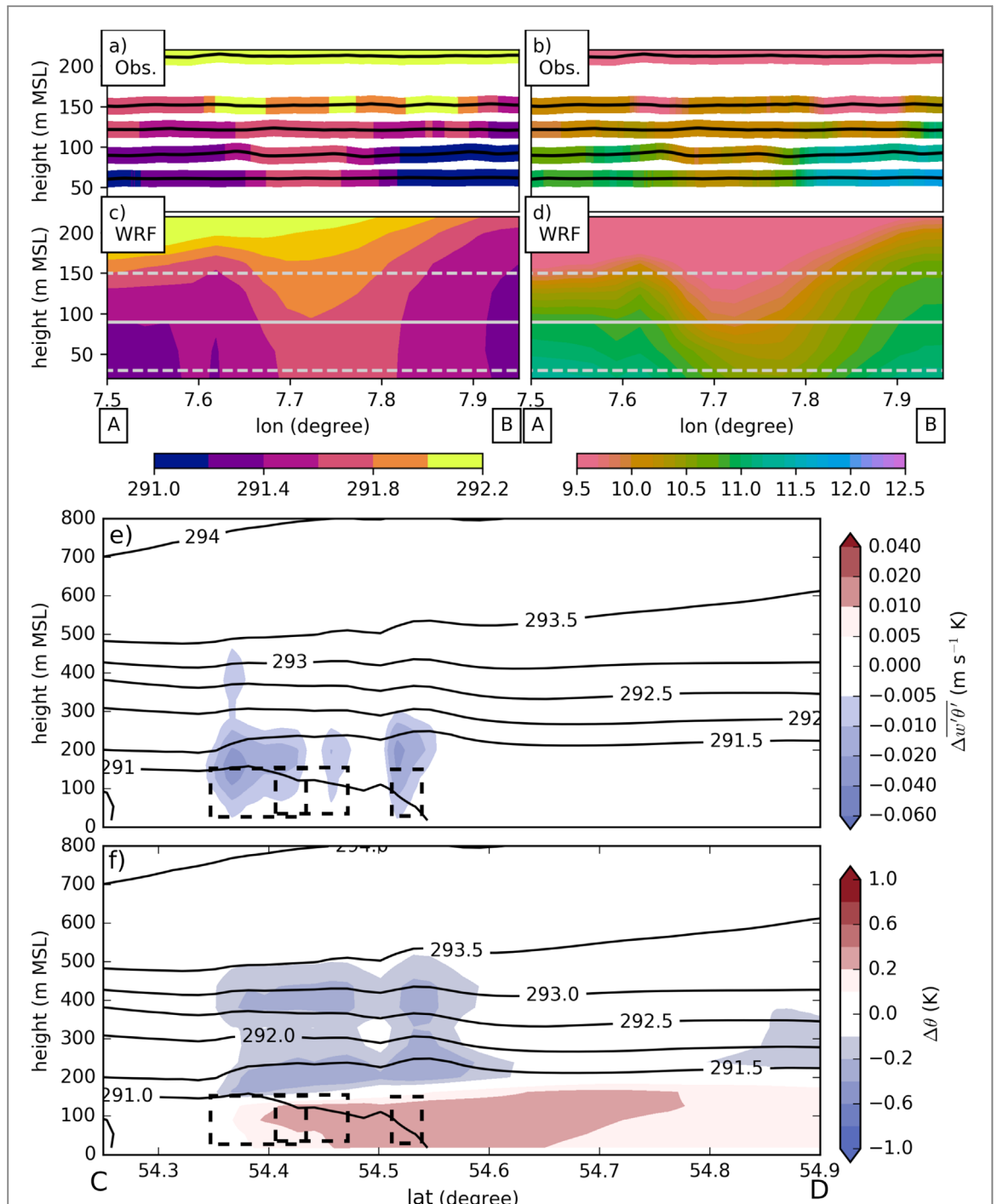
Figure 4. A comparison of observed (a), (b) and simulated (c), (d) potential temperature (a), (c) and water vapor ratio (b), (d) along the vertical cross-section A–B perpendicular to the mean flow. The simulations are shown at 10:00 UTC corresponding to the start of the observations. Further, the difference in sensible heat flux (e) and potential temperature (f) between a WF and NWF simulation is shown averaged from 08:00 UTC to 09:00 UTC. In (e) blue colors indicate an enhanced sensible heat flux downward, whereas in (f) blue contours indicate a cooling and red contours a warming caused by the existence of wind farms Black lines in (a), (b) denote the flight track whereas in (e), (f) they show the potential temperature isolines of the WF simulation. The black and thick dashed boxes in (e), (f) show the rotor area of the three wind farms.

suggest that higher wind speeds would have been necessary to observe a change of temperature at hub height in this case. This assumption is underscored by the observation conducted on the 11 April 2017 (case (c)), where we measured a warming at Godewind with wind speeds of over 10 m s^{-1} at hub height.

The height of the inversion (which is partially driven by SST) determines whether the wind farms warm or cool the atmosphere at hub height in stable conditions. In the cases shown in figures 6(a)–(e) a warming is observed at hub height whereby in figures 6(g)–(i) a cooling of the atmosphere was measured. In the warming cases, a pronounced inversion occurred above hub height accompanied by a less stable layer below, indicating that the enhanced negative heat fluxes in the wakes were stronger above than below the
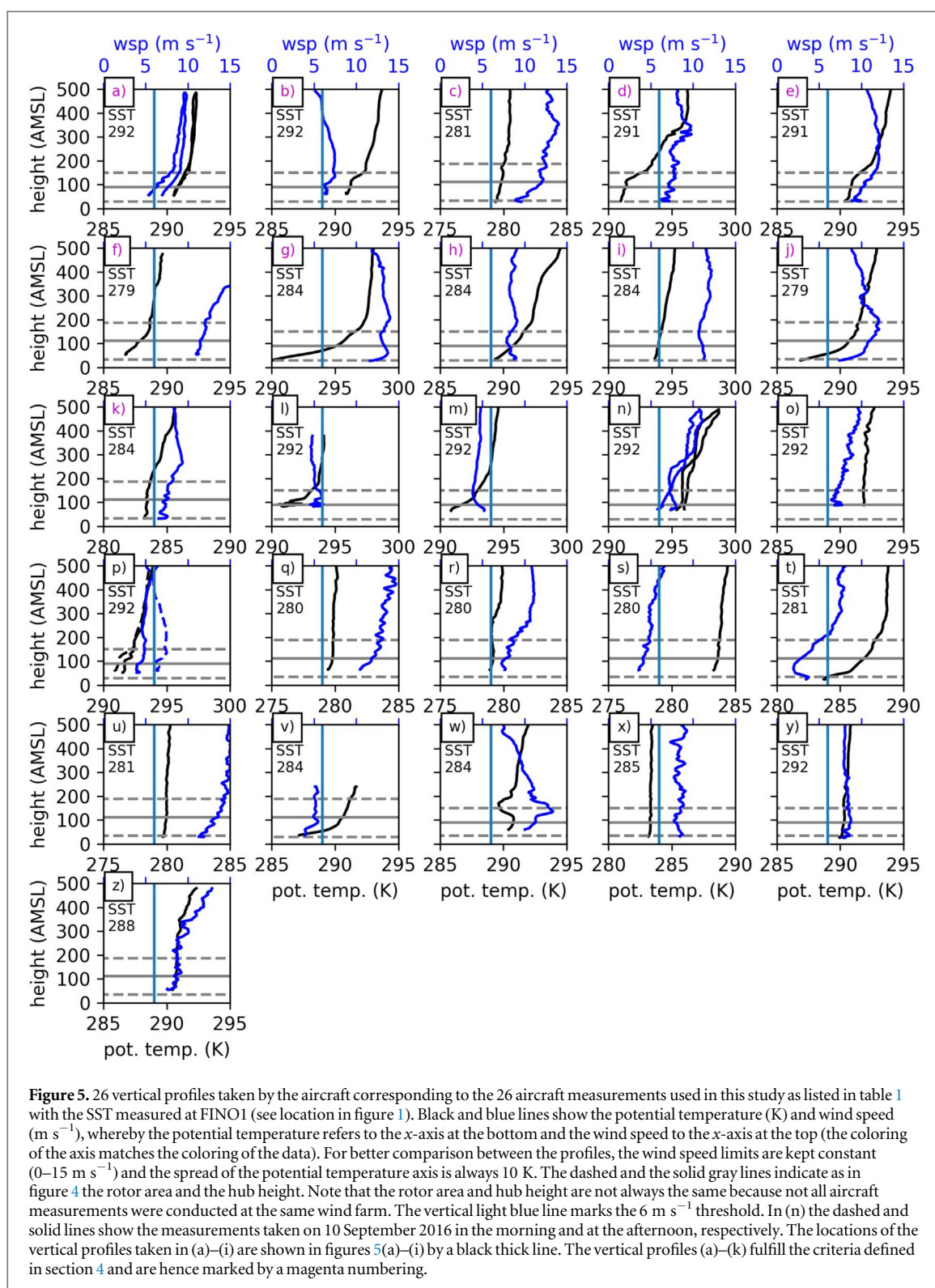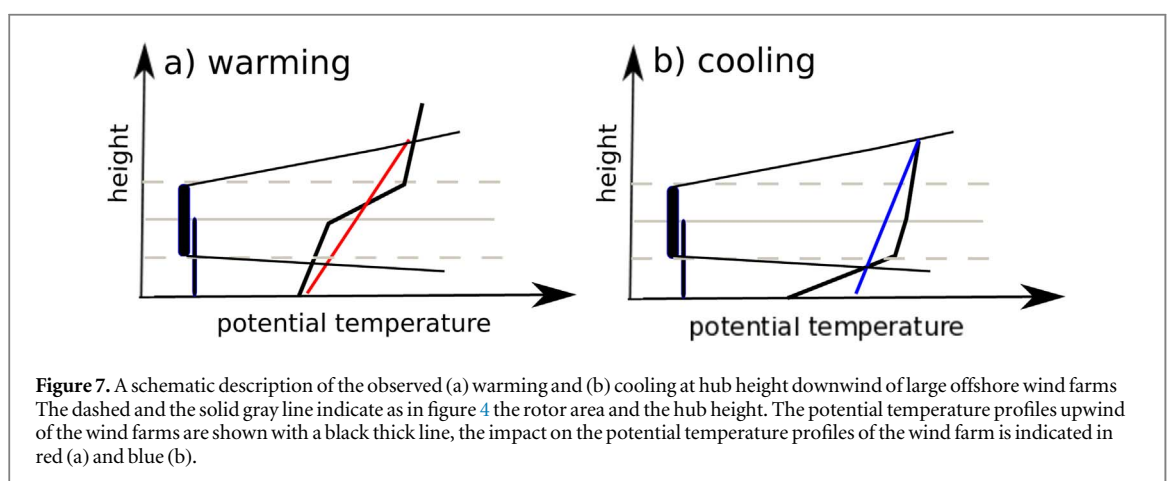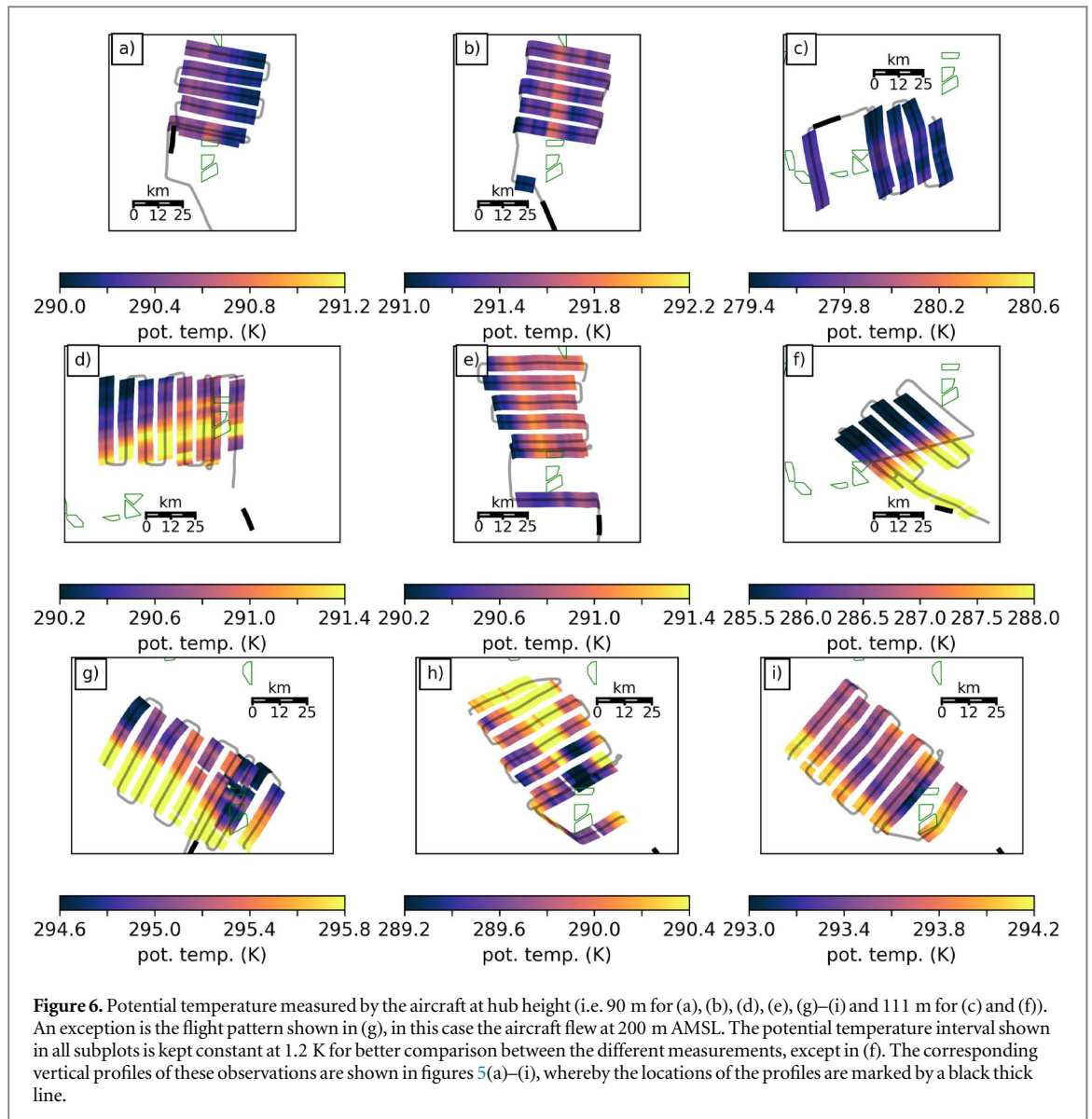
Figure 5. 26 vertical profiles taken by the aircraft corresponding to the 26 aircraft measurements used in this study as listed in table 1 with the SST measured at FINO1 (see location in figure 1). Black and blue lines show the potential temperature (K) and wind speed (m s^{-1}), whereby the potential temperature refers to the x-axis at the bottom and the wind speed to the x-axis at the top (the coloring of the axis matches the coloring of the data). For better comparison between the profiles, the wind speed limits are kept constant (0–15 m s^{-1}) and the spread of the potential temperature axis is always 10 K. The dashed and the solid gray lines indicate as in figure 4 the rotor area and the hub height. Note that the rotor area and hub height are not always the same because not all aircraft measurements were conducted at the same wind farm. The vertical light blue line marks the 6 m s^{-1} threshold. In (n) the dashed and solid lines show the measurements taken on 10 September 2016 in the morning and at the afternoon, respectively. The locations of the vertical profiles taken in (a)–(i) are shown in figures 5(a)–(i) by a black thick line. The vertical profiles (a)–(k) fulfill the criteria defined in section 4 and are hence marked by a magenta numbering.

hub height. As a result, mixing of dry and warm air from above hub height dominates and causes an overall warming at hub height, as schematically indicated in figure 7(a). In contrast, in figures 6(g)–(i) cold SSTs were accompanied by inversions (figures 5(g)–(i)) with their strongest gradients below rotor height, emphasizing that the enhanced negative heat fluxes in the wakes were stronger below than above the hub height, thus causing a net cooling at hub height (figure 7(b)).
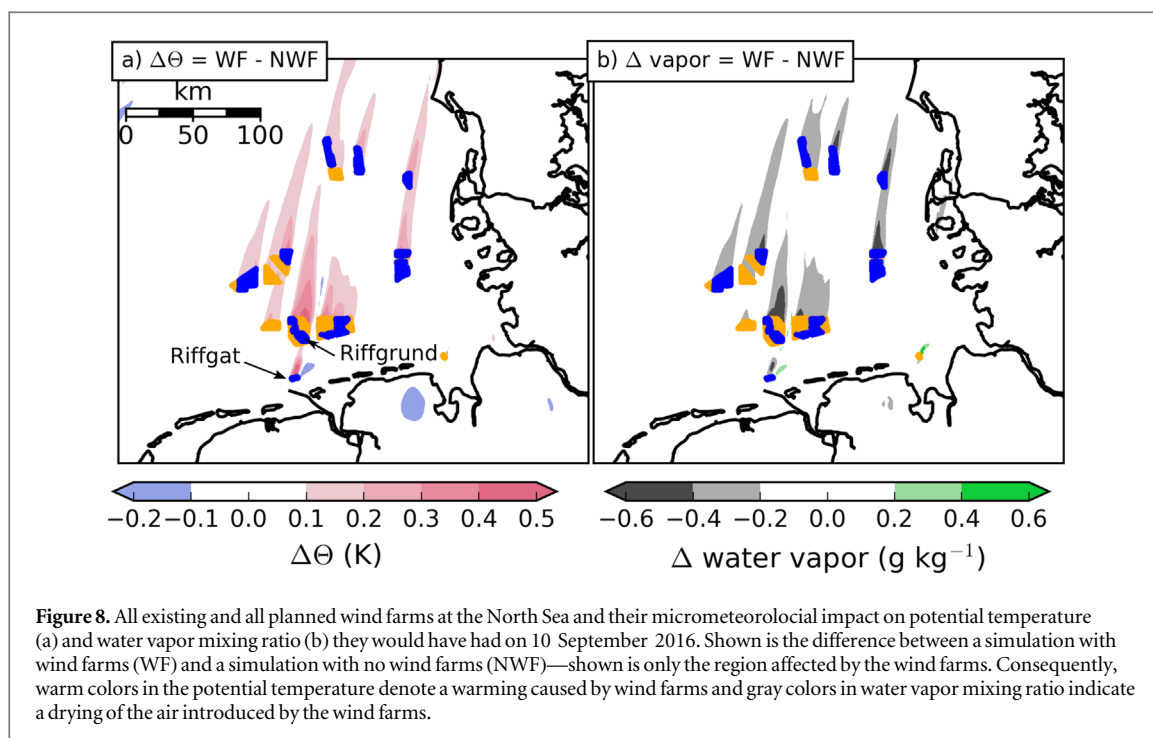
We suggest that these inversions that cause a cooling can be less than 30 m thick. For example, in figure 6(i) we observe a cooling of up to 0.6 K although there is a constant lapse rate within most of the rotor area. However, the SST at FINO1 (see location in figure 1) was 284 K compared to a potential temperature of ≈294 K at 30 m AMSL, indicating that a shallow cold layer close to the ocean surface caused an inversion through the lower portion of the rotor area

Figure 6. Potential temperature measured by the aircraft at hub height (i.e. 90 m for (a), (b), (d), (e), (g)–(i) and 111 m for (c) and (f)). An exception is the flight pattern shown in (g), in this case the aircraft flew at 200 m AMSL. The potential temperature interval shown in all subplots is kept constant at 1.2 K for better comparison between the different measurements, except in (f). The corresponding vertical profiles of these observations are shown in figures 5(a)–(i), whereby the locations of the profiles are marked by a black thick line.

Figure 7. A schematic description of the observed (a) warming and (b) cooling at hub height downwind of large offshore wind farms The dashed and the solid gray line indicate as in figure 4 the rotor area and the hub height. The potential temperature profiles upwind of the wind farms are shown with a black thick line, the impact on the potential temperature profiles of the wind farm is indicated in red (a) and blue (b).

and below, thus cooling due to the enhanced mixing of this cool air within and partly below the rotor area caused the observed cooling.

The observed warming or cooling is decoupled from the drying downwind. For example, we see a warming in figures 6(a)–(e) and cooling in figure 6(i) but in all measurements we see dryer air downwind, meaning that the moisture flux is decoupled from the heat flux—a result in agreement with the findings of Foreman *et al* (2017). However, in nine of the cases

Figure 8. All existing and all planned wind farms at the North Sea and their micrometeorolocial impact on potential temperature (a) and water vapor mixing ratio (b) they would have had on 10 September 2016. Shown is the difference between a simulation with wind farms (WF) and a simulation with no wind farms (NWF)—shown is only the region affected by the wind farms. Consequently, warm colors in the potential temperature denote a warming caused by wind farms and gray colors in water vapor mixing ratio indicate a drying of the air introduced by the wind farms.

that fulfill the criteria for a potential change in temperature at hub height we observed six times a drying and only one time a humidification at hub height. In the remaining two cases we could not measure any change in humidity (case (g), (h)), whereby in case (g) the aircraft was flying at 200m AMSL—a height too high to detect any impact on the humidity (figure 4(b)).

4.2. Future scenario
We have shown that a single wind farm cluster can cause a warming of up to 0.6 K and a drying of $\approx 0.5 \, \mathrm{g \, kg^{-1}}$ at hub height in the MBL according to the observations. Consequently, the overall effect of all wind farms that are operational, approved or under construction is, hence, of interest. To answer this question, we conducted a simulation for 10 September 2016 including all planned and existing wind farms as they are shown in figure 1 (i.e. orange and blue wind farms). For this case study we have measurements along the cross section A–B (figure 3) and could show that the model simulates the vertical and horizontal impact on temperature and humidity, increasing the confidence in the future scenario. Additionally, we had more warming than cooling cases.

The difference between the WF and NWF simulations (figure 8) suggests a similar warming response (within ± 0.1 K) to the case of 10 September 2016 in the presence of more wind farms. For example, downwind of the large wind farm cluster around Riffgrund, a wide area with a warming of up to 0.5 K is found (figure 8), while downwind of the large westernmost cluster the warming is less than 0.3 K. However, not only the size of a wind farm seems to determine the degree of warming. The wind farm Riffgat with only 30 wind turbines causes also a warming of up to 0.5 K.

The simulation suggests a stronger warm air advection aloft at Riffgat and, hence, the inversion at Riffgat is even more pronounced and that in turn allows an even more enhanced downward mixing of warm air. In contrast, the warming at Riffgat is associated with a cooling on the eastern flank of the wake.

While these temperature and moisture changes are novel and may seem consequential when considering the effects of wind farms on local microclimates, it is important to recognize that these are limited effects. The observed local warming and cooling of ± 0.6 K are small compared to the warming that is caused globally by land cover change (LCC) and land management change (LMC). According to Luyssaert *et al* (2014) the warming caused by LCC and LMC is in the order of 1.7 K within the planetary boundary layer. Out of the 26 flights that occurred over a year, an impact on temperature and humidity only occurred when a strong stable stratification existed at turbine hub height or below rotor height. In other cases, without inversions or with inversions located well above turbine rotor height, the enhanced mixing caused by wind farms would not have such an effect.

5. Conclusion

This works gives new insights into micrometeorological impacts of large offshore wind farm clusters by the use of aircraft measurements conducted from September 2016 to October 2017 and mesoscale simulations. The main findings include:

- Large offshore wind farms can have an impact on the MBL. During five measurement flights, the elevation of the inversion in the rotor disk region was such that the potential temperature increased

by up to 0.6 K within the wake of a large offshore wind farm 45 km downwind. This warming was associated with a decrease in the total water vapor mixing ratio by up to $0.5\,\mathrm{g\,kg^{-1}}$. In contrast, a shallow inversion below hub height associated with a cold SST causes a cooling of the same magnitude above and at hub height downwind, as observed during three measurement flights.

- These micrometeorological impacts exist only in case of an inversion below or at rotor area. Only in the presence of such inversions can warmer air be mixed downward by the rotors. Depending on the height of the inversions this process is causing either a warming or cooling at hub height. As an inversion acts as a lid for the water vapor evaporating from the ocean, the water vapor concentration is higher underneath the inversion. Consequently, a breakup of the inversion results in a mixing of dryer air downward and, hence, in dryer air within the wake. This process was observed regardless of a warming or cooling, indicating that the moisture flux is decoupled from the heat flux.

- The mesoscale model simulated the observed warming and drying effect of the wind farm cluster reasonably well. Therefore, we could estimate the overall effect of all planned and existing wind farms on the MBL for the 10 September 2016 case. Even with an increasing number of wind farms, the warming and drying effects remain of the same order of magnitude as in the reference case. The interaction of several wakes resulted in wakes exceeding 100 km in length.

These findings demonstrate that, in some cases, large offshore wind farms can have an impact on the regional microclimate. However, a pure redistribution of moisture and heat has no influence on the regional climate. Only a permanent change in the air–sea interactions could change the regional climate. For example, warmer air over a cold ocean would result in an increased sensible heat flux to the ocean whereby the latent heat flux would transport more water into the atmosphere because of the dryer air within the wake. However, we suggest that these events are rare because a strong inversion at or below hub height is necessary to observe this warming and drying within the wake of large offshore wind farms.

Acknowledgments

ORCID iDs

S K Siedersleben ⓘ https://orcid.org/0000-0002-8467-1471

J K Lundquist ⓘ https://orcid.org/0000-0001-5490-2702

A Platis ⓘ https://orcid.org/0000-0002-9276-3587

S Emeis ⓘ https://orcid.org/0000-0001-6114-6212

References

Abkar M and Porté-Agel F 2015 A new wind-farm parameterization for large-scale atmospheric models *J. Renew. Sustain. Energy* **7** 013121

Armstrong A, Burton R R, Lee S E, Mobbs S, Ostle N, Smith V, Waldron S and Whitaker J 2016 Ground-level climate at a peatland wind farm in Scotland is affected by wind turbine operation *Environ. Res. Lett.* **11** 044024

Baidya Roy S B and Traiteur J J 2010 Impacts of wind farms on surface air temperatures *Proc. Natl Acad. Sci. USA* **107** 17899–904

Barthelmie R J *et al* 2010 Quantifying the impact of wind turbine wakes on power output at offshore wind farms *J. At. Ocean. Technol.* **27** 1302–17

Bilgili M, Yasar A and Simsek E 2011 Offshore wind power development in Europe and its comparison with onshore counterpart *Renew. Sustain. Energy Rev.* **15** 905–15

Christiansen M B and Hasager C B 2005 Wake effects of large offshore wind farms identified from satellite SAR *Remote Sens. Environ.* **98** 251–68

Djath B, Schulz-Stellenfleth J and Cañadillas B 2018 Impact of atmospheric stability on X-band and C-band synthetic aperture radar imagery of offshore windpark wakes *J. Renew. Sustain. Energy* **10** 043301

Emeis S 2010 Meteorological explanation of wake clouds at Horns Rev wind farm *DEWI Mag.* **37** 52–5 (https://dewi.de/dewi/fileadmin/pdf/publications/Magazin_37/07.pdf)

Emeis S, Siedersleben S, Lampert A, Platis A, Bange J, Djath B, Schulz-Stellenfleth J and Neumann T 2016 Exploring the wakes of large offshore wind farms *J. Phys.: Conf. Ser.* **753** 092014

Fitch A C, Olson J B and Lundquist J K 2013 Parameterization of wind farms in climate models *J. Clim.* **26** 6439–58

Fitch A C, Olson J B, Lundquist J K, Dudhia J, Gupta A K, Michalakes J and Barstad I 2012 Local and Mesoscale impacts of wind farms as parameterized in a mesoscale NWP model *Mon. Weather Rev.* **140** 3017–38

Foreman R, Cañadillas B, Neumann T and Emeis S 2017 Measurements of heat and humidity fluxes in the wake of offshore wind turbines *J. Renew. Sustain. Energy* **9** 053304

Hasager C B, Nygaard N G, Volker P J, Karagali I, Andersen S J and Badger J 2017 Wind farm wake: The 2016 Horns Rev photo case *Energies* **10** 317

Hasager C B, Rasmussen L, Peña A, Jensen L E and Réthoré P-E 2013 Wind farm wake: the Horns Rev photo case *Energies* **6** 696–716

Hirth B D and Schroeder J L 2013 Documenting wind speed and power deficits behind a utility-scale wind turbine *J. Appl. Meteorl. Climatol.* **52** 39–46

Huang H-Y and Hall A 2015 Offshore wind development impacts on marine atmospheric environment (http://energy.ca.gov/2016publications/CEC-500-2016-023/CEC-500-2016-023.pdf)

Hunter J D 2007 Matplotlib: a 2d graphics environment *Comput. Sci. Eng.* **9** 90–5

Jiménez P A, Navarro J, Palomares A M and Dudhia J 2015 Mesoscale modeling of offshore wind turbine wakes at the wind farm resolving scale: a composite-based analysis with the Weather Research and Forecasting model over Horns Rev *Wind Energy* **18** 559–66

Lee J C Y and Lundquist J K 2017 Evaluation of the wind farm parameterization in the Weather Research and Forecasting model (version 3.8.1) with meteorological and turbine power data *Geosci. Model Dev.* **10** 4229–44

Lissaman P 1979 Energy effectiveness of arbitrary arrays of wind turbines *J. Energy* **3** 323–8

Luyssaert S *et al* 2014 Land management and land-cover change have impacts of similar magnitude on surface temperature *Nat. Clim. Change* **4** 389

Nakanishi M and Niino H 2004 An improved Mellor–Yamada level-3 model with condensation physics: its design and verification *Bound.-Layer Meteorol.* **112** 1–31

Nygaard N G 2014 Wakes in very large wind farms and the effect of neighbouring wind farms *J. Phys.: Conf. Ser.* **524** 012162

Nygaard N G and Hansen S D 2016 Wake effects between two neighbouring wind farms *J. Phys.: Conf. Ser.* **753** 032020

Pan Y and Archer C L 2018 A hybrid wind-farm parametrization for mesoscale and climate models *Bound.-Layer Meteorol.* **168** 469–95

Platis A *et al* 2018 First *in situ* evidence of wakes in the far field behind offshore wind farms *Sci. Rep.* **8** 2163

Rajewski D A, Takle E S, Lundquist J K, Prueger J H, Pfeiffer R L, Hatfield J L, Spoth K K and Doorenbos R K 2014 Changes in fluxes of heat, H_2O, and CO_2 caused by a large wind farm *Agric. Forest Meteorol.* **194** 175–87

Rajewski D A *et al* 2013 Crop wind energy experiment (CWEX): observations of surface-layer, boundary layer, and mesoscale interactions with a wind farm *Bull. Am. Meteorl. Soc.* **94** 655–72

Rhodes M E and Lundquist J K 2013 The effect of wind-turbine wakes on summertime US midwest atmospheric wind profiles as observed with ground-based doppler lidar *Bound.-Layer Meteorol.* **149** 85–103

Siedersleben S K *et al* 2018 Evaluation of a wind farm parametrization for mesoscale atmospheric flow models with aircraft measurements *Met. Zeit.* accepted (https://doi.org/10.1127/metz/2018/0900)

Skamarock W 2008 A description of the advanced research WRF version 3 *Technical Report* National Center for Atmospheric Research (NCAR) (Boulder, CO) (www2.mmm.ucar.edu/wrf/users/docs/)

Smith C M, Barthelmie R and Pryor S 2013 *In situ* observations of the influence of a large onshore wind farm on near-surface temperature, turbulence intensity and wind speed profiles *Environ. Res. Lett.* **8** 034006

Vautard R, Thais F, Tobin I, Bréon F-M, De Lavergne J-G D, Colette A, Yiou P and Ruti P M 2014 Regional climate model simulations indicate limited climatic impacts by operational and planned European wind farms *Nat. Commun.* **5** ncomms4196

Wang C and Prinn R G 2011 Potential climatic impacts and reliability of large-scale offshore wind farms *Environ. Res. Lett.* **6** 025101

WindEurope 2017 Wind Energy in Europe: Outlook to 2020 (https://windeurope.org/about-wind/reports/wind-energy-in-europe-outlook-to-2020)

Zhang W, Markfort C D and Porté-Agel F 2013 Experimental study of the impact of large-scale wind farms on land-atmosphere exchanges *Environ. Res. Lett.* **8** 015002

Zhou L, Tian Y, Roy S B, Thorncroft C, Bosart L F and Hu Y 2012 Impacts of wind farms on land surface temperature *Nat. Clim. Change* **2** 539–43